
Spontaneous Symmetry Breaking in Data Visualization

Anonymous Author(s)

Affiliation

Address

email

Abstract

1 Data visualization tools are designed for creating low-dimensional representations
2 of data that emphasize structure and suppress noise. However, such non-linear
3 amplifications of structural differences can have side effects like spurious clustering
4 in the widely used t-SNE (Amid and Warmuth [2018]). We present a more general
5 class of spurious structure, namely broken symmetry, defined as visualizations
6 that lack symmetry present in the underlying data. We develop a simple workflow
7 for detection of broken symmetry and give examples of spontaneous symmetry
8 breaking in t-SNE and other well-known algorithms such as GPLVM and kPCA.
9 Our extensive, quantitative study shows that these algorithms frequently break
10 symmetry, thereby highlighting new shortcomings of current visualization tools.

11 1 Motivation

12 *Data visualization* is a core tool in the machine learning toolbox. Data sets are visualized for
13 exploration, to formulate hypotheses and to make modeling decisions. Visualization is commonly
14 used for interpretation of learned models, e.g. visualization of latent variables of a generative model
15 to understand representations. Data visualization is also very useful for debugging. For these
16 applications *faithfulness* is a concern - can we trust the structure revealed in a visualization?

17 Most data of interest is high dimensional, hence can not be directly visualized. Rather, some form of dimensionality reduction
18 is required, which inevitably will lead to loss of information. Popular schemes such as t-SNE [van der Maaten and Hinton, 2008],
19 aim at two or three-dimensional representations that capture both
20 local and global structure in data. Fig. 1 shows a two-dimensional
21 t-SNE visualization of images from the COIL-20 dataset [Nene
22 et al., 1996]; the given example concerns a wooden object on a
23 turntable that is viewed from multiple, equidistant angles forming
24 full 360° rotation. Such an incremental physical rotation leads
25 to a set of images with a simple topological structure which can
26 be quantified by the neighborhood graph. More specifically, we
27 form a graph with the images as nodes and connect neighboring
28 nodes along the rotation path to obtain the graph of a circle. The
29 neighborhood graph presents us with a strong physical symmetry
30 and we naturally expect a visualization of the data to reveal this
31 pattern by a structure which is topologically equivalent to a circle.
32 Evidently, this does not happen: The visualization has broken the symmetry and “invented” a
33 difference between neighboring points that is non-physical.
34
35

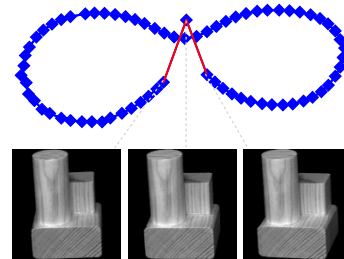


Figure 1: We analyse a set of images of an object subject to a 360° rotation on a turntable. The nearest neighbor graph forms a simple circle, however when the set is visualized using t-SNE the symmetry is lost.

36 The significance of transformations and the ensuing question of symmetry preservation goes beyond
 37 the physical rotations of the COIL data set. Parameterized transformations are key to modern data
 38 augmentation strategies. In this setting, the question of preservation of symmetries in augmented data
 39 sets is related to whether given symmetries are successfully represented by the learning algorithm.

40 **Our contribution** is to identify a new, general class of spurious structures in data visualization,
 41 namely spontaneously broken symmetry, defined as representations that lack symmetry present in
 42 the underlying data. Furthermore, we provide a topological, quantitative measure to detect broken
 43 symmetry (Sec. 2) allowing for a systematic study. Our empirical studies (Sec. 3) show that widely
 44 used visualization techniques break simple symmetries like rotations, hence, challenging the notion
 45 that they conserve global structure.

46 2 Symmetries, Graphs, and Persistent Homology

47 **Symmetry groups.** We consider symmetries. Here, a symmetry
 48 refers to a property of a system that remains unchanged under
 49 a given transformation. The images of the wooden toy in Fig. 1
 50 are formally *equivariant* when the toy is rotated physically on the
 51 turn-table, while the outputs of a deep network for image based
 52 object classification ideally would be invariant (symmetric) under
 53 rotation.

54 Mathematically, such transformations and symmetries are described by Lie groups [Hall, 2015]. A real Lie group is a smooth
 55 differentiable manifold on which points are connected through a
 56 group operation and its inverse. For instance, rotation matrices
 57 form a smooth group with the matrix multiplication group operation.
 58 The unit circle can then be generated by a single unit vector and
 59 its multiplication with all members of the group of rotation
 60 matrices. If the rotation group governs a physical phenomenon
 61 then we expect to observe data along a path that topologically is a circle, disregarding observation
 62 noise.
 63

64 In this paper, we focus on situations where the governing group is known and investigate if the group
 65 structure is preserved by common visualization techniques. This is achieved by verifying if the
 66 topology of the group remains intact under visualizations.

67 **Discrete approximations.** In practice, we only observe a finite number of data points, rather than
 68 the entirety of a group. We can, however, approximate the path spanned by the observations with
 69 a graph, where points are connected if their generating group elements are close under the group
 70 metric. For instance, we may connect rotated images in a graph if their rotation angles are similar as
 71 also described in Sec. 1.

72 **Measuring broken symmetry.** For visualization, we map data to a low-dimensional space (typically \mathbb{R}^2); we let $X = \{x_i\}$ denote data coordinates in this low-dimensional space. We can now
 73 determine if a symmetry has been preserved under visualization by asking if the associated graph can
 74 be recovered from the low-dimensional coordinates. As the graph informs as to which points should
 75 be neighbors, we measure for each set of neighbors the radius of the ball needed to include one in the
 76 other’s neighborhood graph. To compare across methods, we scale all distances by their median
 77

$$B_{\text{median}} = \text{median}_{(x_i, x_j) \in G} (\|x_i - x_j\|), \quad (1)$$

78 where G denotes the graph associated with the generating group. We rely on the median due to its
 79 high breakdown point [Huber, 2004]. We, thus, measure

$$B_{ij} = \frac{\|x_i - x_j\|}{B_{\text{median}}}. \quad (2)$$

80 We can then threshold this measure such that, we say that a symmetry has been broken if $B_{ij} > B_t$
 81 for any pair or equivalently, $\max(B_{ij}) > B_t$. We define $B_{\text{max}} := \max(B_{ij})$. Note that this measure
 82 does not distinguish between one or multiple instances of broken symmetry.

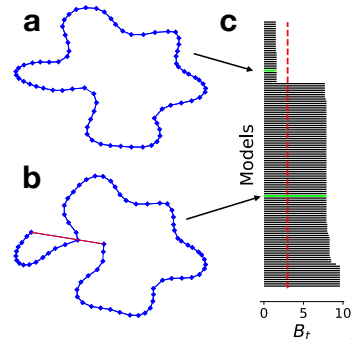


Figure 2: The latent space of a model that preserves symmetry (a) and one that does not (b). (c) A barcode as a function of thresholds B_t .

83 **Persistent homology.** The measure above is linked with *persistent homology* [Hatcher, 2005]. This
84 is a key mathematical tool in topological data analysis that has been shown robust to perturbations
85 of the input data [Cohen-Steiner et al., 2007]. Following Carlsson [2009], we may place balls
86 on each data point with radius ϵ and points falling within this ball defines a neighborhood. This
87 defines a topological space Ω_ϵ . By varying ϵ , we can create multiple topological spaces and let the
88 Betti numbers $b_i(\Omega_\epsilon)$ quantify the structure of the topological space. The number b_0 represents the
89 approximate number of connected components and b_1 the number of circles or holes.

90 In persistent homology, we study a spectrum of neighborhood sizes. For a *known* generating group,
91 we would know its Betti numbers, and may ask which (if any) ϵ yield the given Betti numbers in the
92 visualization point set. This allows us to consider multiple thresholds of our measure (2) of symmetry.

93 **Barcodes.** A broken symmetry is defined by the maximum of the normalized pairwise distances
94 B_{\max} being greater than a threshold B_t . This we can represent by a bar ranging from zero to B_{\max}
95 that visualizes the birth and death of symmetry. Stacking such bars (as in Fig. 2) yields a *barcode*.
96 This lets us inspect the sensitivity of a chosen threshold for multiple models visually as each bar
97 corresponds to a model [Ghrist, 2008]. The ‘sharper’ the transition from short bars to long bars is,
98 the more robust the conclusion is. The barcode in Fig. 2 suggests that a choice of $B_t = 3$ is quite
99 robust as choosing values in the range $B_t = 2$ and $B_t = 8$ yields the same conclusions.

100 For quantitative comparisons across experiments and for simplicity, we have opted for a consistent
101 threshold $B_t = 3$. In all cases, associated barcodes will be provided to quantify the robustness of the
102 chosen threshold in supplements.

103 3 Experiments

104 In our empirical study, we consider four methods representing the spectrum of data visualization
105 techniques:

106 **t-SNE** matches an exponential distribution of pairwise distances in data space with a t-distribution
107 of pairwise distances in the latent space [van der Maaten and Hinton, 2008]. The visualization is
108 controlled by a *perplexity* parameter that quantifies the effective number of neighbors used in the
109 exponential distribution over pairwise distances. This is a randomized model and experiments were
110 performed using scikit learn [Pedregosa et al., 2011].

111 **TriMap** [Amid and Warmuth, 2019] is a recent method that relies on an elaborate triplet weighting
112 scheme such that point triplets are weighted with their pairwise distance before obtaining the final
113 triplet weight $\omega_{ijk} = \zeta_\gamma(\delta + \tilde{\omega}_{ijk}/\omega_{\max})$. Here $\zeta_\gamma(u) = \log(1 + \gamma u)$, where the γ *parameter* is said
114 to place focus on either local or global structure. The method is randomized and experiments were
115 performed using software provided by Amid and Warmuth [2019].

116 **Kernel principle component analysis (kPCA)** [Schölkopf et al., 1998] extends classic PCA through
117 the kernel trick. We use the squared exponential kernel $k(x_i, x_j) = \exp(-\|x_i - x_j\|^2/\lambda)$, which is
118 controlled by the *scale* parameter λ . The model is deterministic and experiments were performed
119 using scikit learn [Pedregosa et al., 2011].

120 **Gaussian process latent variable model (GPLVM)** [Lawrence, 2005] visualizes data us-
121 ing a latent representation with a Gaussian process prior with covariance function $k_{ij} =$
122 $\theta \exp(-1/2\|x_i - x_j\|^2) + \sigma^2 \delta_{ij}$, where x_i, x_j denote latent points. The model is deterministic
123 for a given *initial condition* of the hyperparameters θ and σ^2 , θ_0 and σ_0^2 . Experiments were performed
124 using Pyro [Bingham et al., 2019].

125 **In all experiments**, we vary method parameters over a large range, and randomized methods are
126 repeated multiple times and reported numbers are averages. Experimentally, we focus on the most
127 elementary symmetry of interest: *the rotation group*. We consider images from (1) *COIL-20* where
128 objects are rotated 360° in 72 steps and (2) *MNIST* where we synthetically rotate images with up to
129 360° and 5% Gaussian noise is added. We perform a detailed analysis of each model’s behavior, and
130 quantitatively compare and summarize in Sec. 3.5.

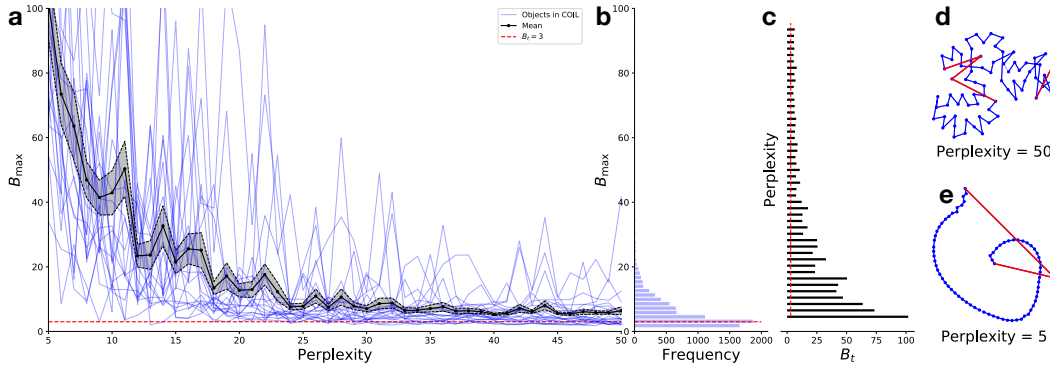


Figure 3: (a) Perplexity parameter space for t-SNE. Each blue line represents the mean over 30 repeats for an object in COIL-20. The dotted, red line marks $B_t = 3$ and the black lines represent mean and standard error over all objects. (b) Histogram of models. (c) Barcode for the mean (black lines in (a)) of objects. (d & e) Latent space in models with perplexities 50 and 5.

131 3.1 t-Distributed Stochastic neighborhood Embedding (t-SNE)

132 To investigate possible symmetry breaking in t-SNE, we fit 30 t-SNE models to images of each
 133 COIL-20 object over a large span of *perplexity* parameters. We measure $B_{\max} = \max B_{ij}$ using (2)
 134 and report averages over the 30 models. These are the blue lines in Fig. 3(a). We see that as perplexity
 135 increase, B_{\max} becomes smaller. This is to be expected as perplexity controls the smoothness of
 136 the t-SNE model. In 73% of all models, we observe broken symmetry ($B_{\max} > 3$). The barcodes
 137 reveal that this percentage is not particular sensitive to the choice of threshold (the red dotted line
 138 correspond to $B_t = 3$). On MNIST, we observe a similar pattern (omitted due to space constraints)
 139 with 96.5% of all models having a broken symmetry.

140 In our experience, t-SNE tends to amplify small gaps in the data, leading to broken symmetry. This
 141 is linked to the ‘spurious clustering’ effect observed by Amid and Warmuth [2018]. We generally
 142 observe that random initialization of t-SNE seems to better preserve symmetries than initialization by
 143 other methods such as PCA or Isomap. This former approach requires multiple restarts and choosing
 144 the embedding with lowest KL divergence.

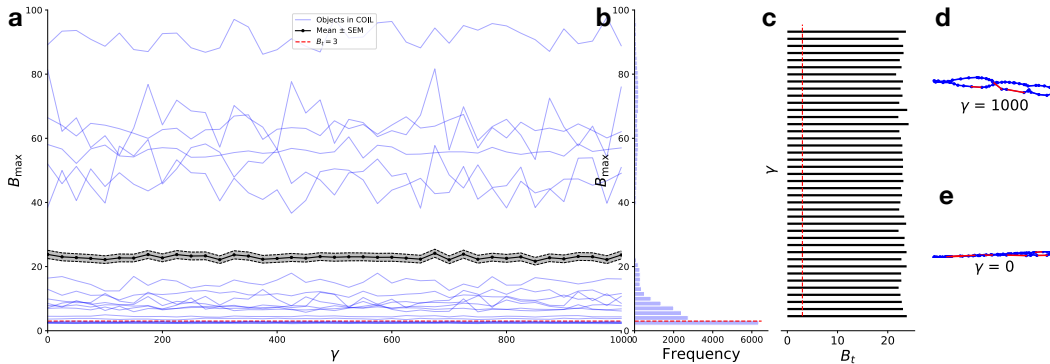


Figure 4: (a) Parameter space for TriMap. Each blue line represents the mean over 30 repeats for an object in COIL-20. The dotted, red line marks $B_t = 3$ and the black lines represent mean and standard error over all objects. (b) Histogram of models. (c) Barcode for the mean (black lines in (a)) of objects. (d) Latent space in model with $\gamma = 1000$. (e) Latent space in model with $\gamma = 0$

145 3.2 TriMap

146 Amid and Warmuth [2019] developed TriMap motivated by the spurious clustering effect in t-SNE,
 147 and we hypothesized that TriMap would lead to less symmetry breaking. However, the evidence in

148 Fig. 4 does not support that conclusion. As before, each blue line shows the average B_{\max} for 30
 149 randomly initialized models for each object in COIL-20 over a wide span of the γ parameter. Here
 150 77% of all models are estimated to show broken symmetry, which is roughly on par with t-SNE. The
 151 barcode indicates that the choice of threshold is robust, though we find some inter-object variability
 152 (see supplements for details). Our findings for MNIST are similar with 93.32% estimated symmetry
 153 breaking.

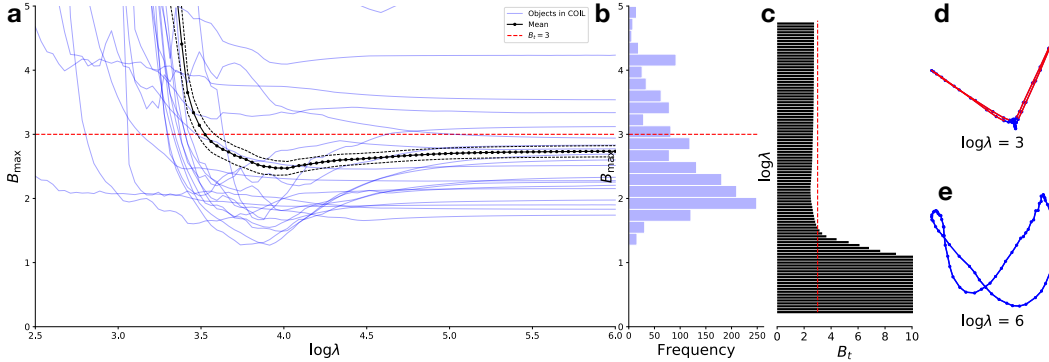


Figure 5: (a) Scale (λ) parameter space for kPCA. Each blue line represents an object in COIL-20. The dotted, red line marks $B_t = 3$ and the black lines represent mean and standard error over all objects. (b) Histogram of models. (c) Barcode for the mean of objects (black lines in (a)). (d) Latent space of model with $\log \lambda = 3$. (e) Latent space of model with $\log \lambda = 6$.

154 3.3 Kernel Principal Component Analysis (kPCA)

155 In kPCA, we examine symmetries as a function of the kernel scale parameter λ . The barcode (Fig. 5)
 156 shows the robustness of the conclusion of preserved symmetry for the mean across COIL-20 objects.
 157 For large values of the scale parameter, the conclusion is robust as B_t can vary, but for smaller values,
 158 our conclusions become sensitive to the specific choice of B_t .

159 In the non-linear regime (small values of λ), B_{median} (1) is driven to a very small values (see example
 160 in Fig. 5d) and thus B_{\max} diverges. In the linear regime (large values of λ), the model approaches
 161 PCA which explains the flattening (see example in Fig. 5e).

162 In 42% of models, we observe broken symmetry and we note that five objects in COIL-20 give rise to
 163 broken symmetries: Object 2 (wooden toy), object 16 (round bottle), object 16 (ceramic vase), object
 164 18 (tea cup) and object 20 (round container). Of these, four are rotationally symmetric in the plane
 165 of rotation, supporting our hypothesis that the additional symmetry can induce symmetry breaking.
 166 More details can be found in the supplements.

167 On MNIST data, the rate of broken symmetries was 7.23%. One possible explanation for this
 168 reduction, is that if PCA on the MNIST data does not induce symmetry breaking then fewer models
 169 will break the symmetry because kPCA converges to PCA in the linear regime.

170 3.4 Gaussian Process Latent Variable Model (GPLVM)

171 We investigated the GPLVM design space by varying the initial values of the kernel hyperparameters,
 172 θ_0 and σ_0^2 all with identical initialization of the latent space (isomap [Tenenbaum, 2000]). In Fig 6a,
 173 θ_0 is fixed and σ_0^2 is varying and in Fig 6b, σ_0^2 is fixed while θ_0 varies. An interesting thing to notice
 174 is while we mostly get consistent results, sometimes a small change in the initial condition induces a
 175 large change in the B_{\max} leading to somewhat complex behavior.

176 We notice that the loss is often an indicator of broken symmetry as we saw with the KL divergence
 177 for t-SNE. If the parameter space contains symmetry-preserving models and symmetry-breaking
 178 models then these generally have lower loss than models that break symmetry.

179 The hyperparameters θ and σ^2 converge to the final values independent of the model preserving
 180 the symmetry. This means that the difference in loss between symmetry-preserving and symmetry-
 181 breaking models must be accounted for by the latent variables. It also means that it is not possible to

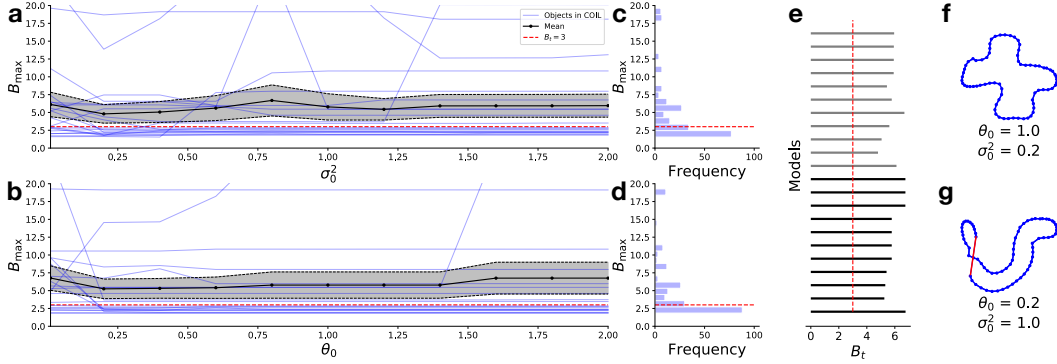


Figure 6: (a-b) Parameter space formed by the initialization values of the hyperparameters, θ_0 and σ_0^2 for GPLVM. Each blue line represents an object in COIL-20. The dotted, red line marks $B_t = 3$ and the black lines represent mean and standard error over all objects. (a) Parameter space in σ_0^2 with fixed θ_0 . (b) Parameter space in θ_0 with fixed σ_0^2 . (c) Histogram of models in a. (d) Histogram of models in b. (e) Barcode for the mean of objects (black lines in (a) and (b)). (f) Latent space of model with $\theta_0 = 1$ and $\sigma_0^2 = 0.2$. (g) Latent space of model with $\theta_0 = 0.2$ and $\sigma_0^2 = 0.2$.

182 detect a broken symmetry from the optimized hyperparameters but rather, one have to consider the
 183 latent variables to detect a broken symmetry.

184 Like in kPCA, we find broken symmetries in the most symmetric objects. In the GPLVM, this is
 185 linked to the choice of initialization of the latent space. More in supplements.

186 Overall, we found broken symmetries in 65.48% of the models and similarly, in MNIST, the rate was
 187 46.32%. The supplements contains parameter spaces for additional datasets.

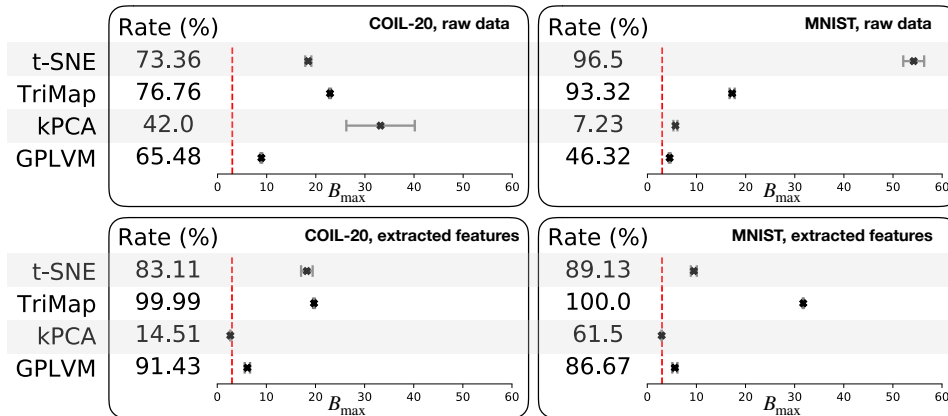


Figure 7: Each pane shows the rate of broken symmetries in percent at $B_t = 3$ with the mean and standard error plotted displayed on the axis for t-SNE, TriMap, kPCA, and GPLVM. *Top, left pane*) Summary of results on COIL-20. *Top, right pane*) Summary of results on MNIST. *Bottom, left pane*) Summary of results on features extract from COIL-20 using ResNet-18. *Bottom, right pane*) Summary of results on features from MNIST using ResNet-18.

188 3.5 Summary of experiments

189 We found broken symmetry in all models with a high prevalence as summarized in Fig. 7. The details
 190 are found in Sec. 3.1-3.4. Note that we did not tune the parameters but varied important parameters
 191 across large ranges and used default parameters for others.

192 We note that all objects in COIL-20 are indeed symmetric in data space according to our estimator.
 193 One may expect that high-level features may be less susceptible to broken symmetry than raw
 194 data. We investigate this using ResNet18 [He et al., 2015] to extract features and investigated

195 the prevalence here. We found no broken symmetries in the extracted features and no consistent,
196 significant difference when looking at symmetry in the models trained on extracted features. We
197 noticed that the most symmetric objects generally experienced more broken symmetry across models.

198 4 Related Works

199 **Data visualization** is important at many steps in the machine learning process. Visualization is used
200 exploratively to form hypotheses [Arora et al., 2018], for understanding latent representations in
201 supervised learning [Esteva et al., 2017] and generative models [Frid-Adar et al., 2018].

202 The desiderata of visualization are discussed by Kaski et al. [2003] and Venna et al. [2010], who argue
203 that visualizations should be trustworthy, meaning that samples appearing similar (e.g., neighbors) in
204 the visualization should be similar in a physical sense. Also, they point out that data points close
205 in a physical sense should be close in visualization. They noted the similarity with the concepts of
206 precision and recall in information retrieval. Our concept of broken symmetry is related to the “recall”
207 dimension, i.e., data that are physical neighbors, should also be visualized as such. The precision
208 and recall criteria together measure the faithfulness of the visualization, see also Najim [2014] for a
209 related quantitative measure of the preservation of neighborhood relations in visualizations.

210 The immensely popular visualization scheme t-SNE [van der Maaten and Hinton, 2008] is con-
211 structed with the aim of representing both global and local structure. The original motivation for
212 t-SNE included a critique of its predecessor SNE [Hinton and Roweis, 2003] for creating crowded
213 visualizations, i.e., visualizations that did not show a clear separation of known clusters. Crowding is
214 closely related to the trustworthiness concept of Kaski et al. [2003], Venna et al. [2010]. By using a
215 long-tailed distribution of the representations, t-SNE aims to fix the crowding problem. However,
216 this emphasis of local dissimilarity comes at a price as noted in Linderman and Steinerberger [2017],
217 simple manifolds like lines and sheets are broken apart in clusters. These clustering problems are
218 examples of broken symmetry in our definition. Motivated by the problem of over-fitting cluster
219 structure Amid and Warmuth [2019] proposed TriMap. We observed, however, that TriMap cannot
220 heal the problem of broken symmetry.

221 For the detection of symmetries, we employed topological data analysis [Carlsson, 2009], specifically
222 persistent homology. Using this, we examined all values of thresholds simultaneously rather than
223 study just a single threshold. Conveniently, Cohen-Steiner et al. [2007] showed that the persistent
224 homology tool is robust under perturbations of the data. Pokorny et al. [2012] used persistent homology
225 in its classical form whereas we have adapted it slightly as we knew which Betti numbers were
226 required to preserve the symmetry. Our work exploits the coordinate and deformation invariances
227 in topology and these properties aid in detecting symmetries as various deformations of the “circle”
228 graph.

229 5 Discussion

230 We have investigated to which extend common visualization techniques are able to preserve simple
231 symmetries, and have largely found the answer to be negative.

232 5.1 Empirical findings

233 We have investigated four popular algorithms that also represent different branches of the literature,
234 namely t-SNE [van der Maaten and Hinton, 2008], TriMap [Amid and Warmuth, 2019], kPCA
235 [Schölkopf et al., 1998] and the GPLVM [Lawrence, 2005]. We have performed a systematic study
236 of the influence of parameter choices in these methods by training more than 85.000 models over a
237 wide parameter span. To quantitatively summarize these models’ performance, we have introduced a
238 simple scheme for detecting whether known symmetries are broken. Tools from persistent homology
239 verify that this scheme is generally reliable, with some deviations for kPCA (see below).

240 **t-SNE** was found to be particularly sensitive to local optima and generally we found a need for
241 multiple restarts. Fortunately, we generally observe that smaller KL reported values imply less
242 symmetry breaking. Even with such mechanisms in place, we still see an overwhelming number of
243 broken symmetries. Symmetry breaking can, to some extend, be reduced by increasing the perplexity
244 parameter, but this also limits the flexibility and expressivity of the model.

245 **TriMap**, which was developed in part to alleviate problems with t-SNE, overall had comparable
246 behavior to t-SNE with regards to broken symmetry. The γ parameter, that controls the trade-off
247 between capturing local or global structure, was found to have practically no effect with regards to
248 symmetry breaking. We did not expect this, but have manually verified that broken symmetry is
249 prevalent across large spans of γ .

250 **kPCA** was in a sense the most successful method according to our estimator. Kernel PCA, however,
251 has a tendency to collapse points on to each other when mapping only two latent dimensions in
252 the non-linear regime leading to strong symmetry breaking. On the other hand, kPCA reduces to
253 conventional PCA in the limit of large kernel length scales, showing less symmetry breaking.

254 **GPLVM** was generally found to be sensitive to choice of initial parameters. While we have found it
255 helpful to consider multiple restarts and choosing the model with highest likelihood, we have found
256 broken symmetry to be rather prevalent.

257 **High-level features.** One could suspect that symmetries are broken more commonly when working
258 with raw data than with high-level abstract features, e.g., as those extracted by deep neural networks.
259 We found no broken symmetries directly in the high-level features though when applying visualization
260 algorithms, the prevalence was indeed high.

261 **Summary.** Our general finding is that symmetries are broken consistently across the studied meth-
262 ods. It is generally possible to manually tweak parameters to enforce that a known symmetry remains
263 intact, but such strategies are not possible when the symmetry is unknown¹, e.g. for knowledge
264 discovery. We also note that default parameters of publicly available implementations of the studied
265 methods generally perform poorly with regards to broken symmetry.

266 5.2 Faithful representations

267 At the heart of our study is the quest for *faithful representations*, i.e. representations that reflect
268 the underlying physics of the data generating process. These have wider applicability than just
269 visualization as studied here. For instance, a representation that is not faithful will most likely not
270 result in a fair prediction. A broken symmetry can be viewed as model that violates the Lipschitz
271 continuity condition. *Individual fairness* [Dwork et al., 2011] can then no longer be ensured as
272 *similar individuals should be treated similarly*.

273 Similar statements can be made for interpretable models, where ‘almost discontinuous’ models are
274 generally difficult to interpret. From a purely predictive point of view, it is strictly not required that
275 representations are faithful, though there is some evidence in that direction [Rieger et al., 2019].

276 Finally, we note that visualization may be particularly sensitive to symmetry breaking as we tend
277 to embed onto \mathbb{R}^2 . While it is well-known that only few graphs (namely the *planar* ones) can be
278 embedded in \mathbb{R}^2 , then *all* graphs can be embedded in \mathbb{R}^3 [Nishizeki and Chiba, 1988]. This suggest
279 that symmetries are likely to be broken when data is forced onto a two-dimensional view, and indeed
280 our experiments indicate that symmetry breaking is less frequent when embedding into three or more
281 dimensions (see supplements).

282 5.3 Concluding remarks

283 We have here pointed to a previously unnoticed problem in visualizations, namely *broken symmetries*.
284 Through a systematic study of more than 85.000 trained models, we have found an alarming rate at
285 which even the most simple symmetries are spontaneously broken during data visualizations. This
286 suggest a need for both new methods that can reliably visualize high-dimensional data, but also for
287 more systematic and quantitative evaluations of visualization techniques.

288 We have purposefully not investigated more complex symmetries as these raise complications that
289 are beyond existing techniques; for instance, the two-dimensional torus is mathematically impossible
290 to embed in \mathbb{R}^2 without breaking the underlying symmetry. This calls for visualization techniques
291 that embed onto curved surfaces in order to preserve symmetries, just as we use a sphere when we
292 visualize global geoinformatics patterns.

¹It should be emphasized that while we consider known symmetries, we only do so in order to make quantitative statements.

293 6 Broader impact

294 Our work demonstrates the alarmingly high prevalence of misrepresentation of symmetries in data
295 visualization which is integral in machine learning. Though we have focused on visualizations, our
296 method does not restrict itself to two dimensions and our considerations are generally applicable to
297 dimensionality reductions and latent variable models in any latent dimensionality.

298 Our main consideration concerns how the broken symmetry might affect down-stream decision-
299 making. As also hinted to in the main body of paper, individual fairness (*similar individuals should*
300 *be treated similarly* [Dwork et al., 2011]) might be breached in models that do not preserve the
301 symmetry. Both a broken symmetry and breached individual fairness are essentially violations of the
302 Lipschitz continuity condition.

303 The consequence of this is that two similar individuals get mapped to different areas of the latent space.
304 This is a one to many mapping from data space to latent space and might lead to an overrepresentation
305 if the latent space is sampled from. This solely emphasizes the importance of visualizations and
306 models being faithful in general.

307 References

- 308 Ehsan Amid and Manfred K. Warmuth. A more globally accurate dimensionality reduction method
309 using triplets. *arXiv:1803.00854 [cs]*, March 2018.
- 310 Ehsan Amid and Manfred K. Warmuth. TriMap: Large-scale Dimensionality Reduction Using
311 Triplets. *arXiv:1910.00204 [cs, stat]*, October 2019.
- 312 Sanjeev Arora, Wei Hu, and Pravesh K Kothari. An analysis of the t-sne algorithm for data visualiza-
313 tion. *arXiv preprint arXiv:1803.01768*, 2018.
- 314 Eli Bingham, Jonathan P. Chen, Martin Jankowiak, Fritz Obermeyer, Neeraj Pradhan, Theofanis
315 Karaletsos, Rohit Singh, Paul Szerlip, Paul Horsfall, and Noah D. Goodman. Pyro: Deep universal
316 probabilistic programming. *The Journal of Machine Learning Research*, 20(1):973–978, January
317 2019. ISSN 1532-4435.
- 318 Gunnar Carlsson. Topology and data. *Bulletin of the American Mathematical Society*, 46(2):255–308,
319 January 2009. ISSN 0273-0979. doi: 10.1090/S0273-0979-09-01249-X.
- 320 David Cohen-Steiner, Herbert Edelsbrunner, and John Harer. Stability of Persistence Diagrams.
321 *Discrete & Computational Geometry*, 37(1):103–120, January 2007. ISSN 1432-0444. doi:
322 10.1007/s00454-006-1276-5.
- 323 Cynthia Dwork, Moritz Hardt, Toniann Pitassi, Omer Reingold, and Rich Zemel. Fairness Through
324 Awareness. *arXiv:1104.3913 [cs]*, November 2011.
- 325 Andre Esteva, Brett Kuprel, Roberto A Novoa, Justin Ko, Susan M Swetter, Helen M Blau, and
326 Sebastian Thrun. Dermatologist-level classification of skin cancer with deep neural networks.
327 *Nature*, 542(7639):115–118, 2017.
- 328 Maayan Frid-Adar, Idit Diamant, Eyal Klang, Michal Amitai, Jacob Goldberger, and Hayit Greenspan.
329 Gan-based synthetic medical image augmentation for increased cnn performance in liver lesion
330 classification. *Neurocomputing*, 321:321–331, 2018.
- 331 Robert Ghrist. Barcodes: The persistent topology of data. *Bulletin of the American Mathematical*
332 *Society*, 45(1):61–75, 2008. ISSN 0273-0979, 1088-9485. doi: 10.1090/S0273-0979-07-01191-3.
- 333 Brian C. Hall. *Lie Groups, Lie Algebras, and Representations: An Elementary Introduction*. Graduate
334 Texts in Mathematics. Springer International Publishing, second edition, 2015. ISBN 978-3-319-
335 13466-6. doi: 10.1007/978-3-319-13467-3.
- 336 Allen Hatcher. *Algebraic topology*. Cambridge University Press, 2005.
- 337 Kaiming He, Xiangyu Zhang, Shaoqing Ren, and Jian Sun. Deep Residual Learning for Image
338 Recognition. *arXiv:1512.03385 [cs]*, December 2015.

- 339 Geoffrey E. Hinton and Sam T. Roweis. Stochastic neighbor embedding. In *Advances in Neural*
340 *Information Processing Systems*, pages 857–864, 2003.
- 341 Peter J Huber. *Robust statistics*, volume 523. John Wiley & Sons, 2004.
- 342 Samuel Kaski, Janne Nikkilä, Merja Oja, Jarkko Venna, Petri Törönen, and Eero Castrén. Trust-
343 worthiness and metrics in visualizing similarity of gene expression. *BMC bioinformatics*, 4:48,
344 October 2003. ISSN 1471-2105. doi: 10.1186/1471-2105-4-48.
- 345 Neil D. Lawrence. Probabilistic Non-linear Principal Component Analysis with Gaussian Process
346 Latent Variable Models. *Journal of Machine Learning Research*, page 34, 2005.
- 347 George C. Linderman and Stefan Steinerberger. Clustering with t-SNE, provably. *arXiv:1706.02582*
348 *[cs, stat]*, June 2017.
- 349 Safa A Najim. Information visualization by dimensionality reduction: a review. *Journal of Advanced*
350 *Computer Science & Technology*, 3(2):101, 2014.
- 351 Sameer A Nene, Shree K Nayar, and Hiroshi Murase. Columbia Object Image Library (COIL-20).
352 *Technical Report CUUCS-006-96*, page 6, 1996.
- 353 Takao Nishizeki and Norishige Chiba. *Planar graphs: Theory and algorithms*. Elsevier, 1988.
- 354 F. Pedregosa, G. Varoquaux, A. Gramfort, V. Michel, B. Thirion, O. Grisel, M. Blondel, P. Pretten-
355 hofer, R. Weiss, V. Dubourg, J. Vanderplas, A. Passos, D. Cournapeau, M. Brucher, M. Perrot, and
356 E. Duchesnay. Scikit-learn: Machine learning in Python. *Journal of Machine Learning Research*,
357 12:2825–2830, 2011.
- 358 Florian T. Pokorny, Hedvig Kjellström, Danica Kragic, and Carl Ek. Persistent Homology for
359 Learning Densities with Bounded Support. In F. Pereira, C. J. C. Burges, L. Bottou, and K. Q.
360 Weinberger, editors, *Advances in Neural Information Processing Systems 25*, pages 1817–1825.
361 Curran Associates, Inc., 2012.
- 362 Laura Rieger, Chandan Singh, W James Murdoch, and Bin Yu. Interpretations are useful: penalizing
363 explanations to align neural networks with prior knowledge. *arXiv preprint arXiv:1909.13584*,
364 2019.
- 365 Bernhard Schölkopf, Alexander Smola, and Klaus-Robert Müller. Nonlinear Component Analysis as
366 a Kernel Eigenvalue Problem. *Neural Computation*, 10(5):1299–1319, July 1998. ISSN 0899-7667,
367 1530-888X. doi: 10.1162/089976698300017467.
- 368 J. B. Tenenbaum. A Global Geometric Framework for Nonlinear Dimensionality Reduction. *Science*,
369 290(5500):2319–2323, December 2000. ISSN 00368075, 10959203. doi: 10.1126/science.290.
370 5500.2319.
- 371 Lauren van der Maaten and Geoffrey Hinton. Visualizing Data using t-SNE. *Journal of machine*
372 *learning research*, pages 2579–2605, 2008.
- 373 Jarkko Venna, Jaakko Peltonen, Kristian Nybo, Helena Aidos, and Samuel Kaski. Information
374 Retrieval Perspective to Nonlinear Dimensionality Reduction for Data Visualization. *Journal of*
375 *Machine Learning Research*, 11(13):451–490, 2010. ISSN 1533-7928.